Comprehensive imaging and Raman spectroscopy of carbonate globules from martian meteorite ALH 84001 and a terrestrial analogue from Svalbard. Meteorit. Planet. Sci. 42(9), 1549-156...

ARTICLE · AUGUST 2007

DOI: 10.1111/j.1945-5100.2007.tb00590.x

The Meteoritical Society

Meteoritics & Planetary Science 42, Nr 9, 1549–1566 (2007)
Abstract available online at http://meteoritics.org

Comprehensive imaging and Raman spectroscopy of carbonate globules from Martian meteorite ALH 84001 and a terrestrial analogue from Svalbard

A. STEELE[1*], M. D. FRIES[1], H. E. F. AMUNDSEN[2], B. O. MYSEN[1], M. L. FOGEL[1], M. SCHWEIZER[1], and N. Z. BOCTOR[1]

[1]Geophysical Laboratory, Carnegie Institution of Washington, 5251 Broad Branch Road, Washington, D.C. 20015, USA
[2]Physics of Geological Processes (PGP), University of Oslo, P.O. Box 1048 Blindern, N-0316 Oslo, Norway
[*]Corresponding author. E-mail: asteele@ciw.edu

(Received 09 May 2006; revision accepted 18 March 2007)

Abstract–We report a comprehensive imaging study including confocal microRaman spectroscopy, scanning electron microscopy (SEM), and 3-D extended focal imaging light microscopy of carbonate globules throughout a depth profile of the Martian meteorite Allan Hills (ALH) 84001 and similar objects in mantle peridotite xenoliths from the Bockfjorden volcanic complex (BVC), Svalbard. Carbonate and iron oxide zoning in ALH 84001 is similar to that seen in BVC globules. Hematite appears to be present in all ALH 84001 carbonate-bearing assemblages except within a magnesite outer rim found in some globules. Macromolecular carbon (MMC) was found in intimate association with magnetite in both ALH 84001 and BVC carbonates. The MMC synthesis mechanism appears similar to established reactions within the Fe-C-O system. By inference to a terrestrial analogue of mantle origin (BVC), these results appear to represent the first measurements of the products of an abiotic MMC synthesis mechanism in Martian samples. Furthermore, the ubiquitous but heterogeneous distribution of hematite throughout carbonate globules in ALH 84001 may be partly responsible for some of the wide range in measured oxygen isotopes reported in previous studies. Using BVC carbonates as a suitable analogue, we postulate that a low temperature hydrothermal model of ALH 84001 globule formation is most likely, although alteration (decarbonation) of a subset of globules possibly occurred during a later impact event.

INTRODUCTION

Carbonate minerals in Martian meteorites, and in particular Allan Hills (ALH) 84001, bear witness to the processing of volatile and biologically relevant compounds (CO_2 and H_2O) on Mars. There is a pool of macromolecular carbon (MMC), both within the carbonate globules and along fracture surfaces of the host pyroxene of ALH 84001 that is indigenous to the meteorite (McKay et al. 1996; Jull et al. 1998). In the debate as to whether relic Martian life exists in ALH 84001, the source of high molecular mass organic material, particularly polyaromatic hydrocarbons (PAHs), has been the focus of significant research (McKay et al. 1996; Bada et al. 1998; Becker et al. 1999; Stephan et al. 2003). Jull et al. (1998) ascribe 80% of the organic material in ALH 84001 to terrestrial contamination and 20% as an indigenous, undefined MMC species. The nature, provenance, and formation mechanisms of this indigenous MMC in both the matrix and the carbonate globules remains unknown, although both biogenic and meteoritic infall origins have been suggested (McKay et al. 1996; Becker et al. 1999).

Existing analyses describe the provenance of MMC only in poorly defined spatial locations such as the carbonates within the host rock or as a comparison between carbonate rich areas and the matrix (Bada et al. 1998; Becker et al. 1999; Jull et al. 1998). Although in situ techniques were used in an attempt to determine the spatial distribution of MMC with respect to the surrounding mineralogy, these studies either failed to detect carbon (Treiman et al. 1998b; Bell et al. 1999; Cooney et al. 1999), or if carbon species were detected, they were ascribed to contamination (Stephan et al. 2003). Only the studies of Flynn et al. (1997, 1998) placed carbonaceous material within the interior and rims of a small number of carbonate globules, sometimes associated with magnetite. The authors did not, however, propose a mechanism for MMC formation.

No systematic studies of ALH 84001 from the external fusion crust to the core of the meteorite have been conducted.

McKay et al. (1996) reported the analysis of a depth profile to 1.2 mm below the surface on a single sample from the meteorite. Other studies have been performed on a very limited subset of samples taken from random points within ALH 84001. We report results from confocal microRaman imaging spectroscopy coupled with 3-D montage light microscopy and scanning electron microscopy (SEM) to study carbonate globules, disseminated (slab) carbonates, and features within the bulk rock of ALH 84001. These measurements were conducted on fresh fracture surfaces throughout five allocations of ALH 84001. These samples constitute a complete depth profile from fusion crust to the center of the meteorite.

Comparative studies were undertaken on carbonate globules contained in spinel lherzolite xenoliths from the Bockfjord Volcanic Complex (BVC) on Svalbard. These xenoliths occur in volcanic centers formed by subglacial eruptions ~1 Myr ago. The BVC eruptive centers have a range of different carbonate deposits (Amundsen 1987), including magnesite globules similar to those found in ALH 84001. These carbonates occur in both basalt vesicles and in mantle xenoliths (Treiman et al. 2002). While the basalt-hosted carbonate globules likely formed from percolating hydrothermal or meteoric fluids, a range of carbonate globules in BVC xenoliths occur both as trapped inclusions within mantle minerals and in pockets between mineral grains, and are interpreted to have been deposited by primary mantle fluids (Amundsen 1987). Although the carbon and oxygen data on calcite ($\delta^{13}C_{PDB}$ = −2‰, $\delta^{18}O_{PDB}$ = −9‰) and dolomite ($\delta^{13}C_{PDB}$ = −1‰, $\delta^{18}O_{PDB}$ = −5‰) analyzed by Mojzsis et al. (1999) could suggest formation from crustal or meteoric fluids, the lherzolite-hosted carbonate globules studied here show a textural setting and carbon isotope composition ($\delta^{13}C_{PDB}$ = −6‰) (Steele et al. 2005), indicating formation from cooling of primary mantle CO_2-rich fluids.

MATERIALS AND METHODS

Analyses were conducted on ALH 84001 samples 380, 357, 347, 336, and 332, which represented a depth profile through the meteorite. Fusion crust was present in 332, 357, and 380 (these samples ~0.5 mm of the surface); sample 336 was located ~1.5 cm from fusion crust. Sample 347 originated from the center of the meteorite (3 cm from the fusion crust). Samples were removed from curation vials and placed onto clean glass slides. No further mounting agents were used except in the case of one sample from the 347 allocation, which was mounted using mounting putty to place a target globule into a single focal depth field.

Svalbard xenolith samples were obtained during the Arctic Mars Analogue Svalbard Expeditions (AMASE 2003 and 2004) to the Sverrefjell volcano, Bockfjorden volcanic complex (BVC), Svalbard. Analyses were conducted on thin sections and freshly fractured surfaces. All analyses were completed on instrumentation present at Carnegie Institution of Washington.

Raman Analysis

Raman spectra and images were collected from carbonate globules and their rims, slab carbonates, and matrix features in ALH 84001 and on carbonate globules within cracks and inclusions in the BVC xenoliths. Raman imaging was performed using a Witec α-scanning near-field optical microscope (SNOM) which has been customized to incorporate confocal Raman spectroscopy imaging. The excitation source was a frequency-doubled solid-state YAG laser (532 nm) operating between 0.3 and 1 mW output power, as measured at the sample using a laser power meter. Objective lenses used included a 100× super long working objective (SLWD) and a 20× long working distance (LWD). The lateral resolution of the instrument is as small as 360 nm in air when using the 100× SLWD objective, or 810 nm when using the 20× objective. A 50 μm optical fiber acting as the confocal pin hole was used to transmit the laser light and Raman signal. Spectra were collected on a Peltier-cooled Marconi 40-11 CCD chip, after passing through a f/4 300 mm focal length imaging spectrometer typically using a 600 lines/mm grating.

This instrument is capable of operating in several modes. Typically, the imaging and single spectra modes were used during this study. For single spectrum acquisition, integration times of 30 s per accumulation over 10 accumulations were used to allow verification of weak spectral features. Raman imaging was conducted by taking a Raman spectrum at each pixel within a field of interest determined by light microscopy. A sequential spectral acquisition mode was used during laser heating experiments (see below).

A cosmic ray reduction routine was used to reduce the effects of stray radiation on Raman images, as was image thresholding to reject isolated bright pixels. Fluorescence effects were inhibited by the use of specific peak fitting in place of spectral area sums and by the confocal optics used in this instrument. In a typical scan at 100× of a 30 μm^2 area, 100 × 100 pixels were scanned amounting to 10,000 separate and spatially aligned Raman spectra. Average spectra were then generated from areas of interest to ascertain parameters, such as peak intensity, peak center, and peak width. All of these parameters could then be mapped across the analysis area.

A number of areas were analyzed in each ALH 84001 sample, including the carbonate globules, diffuse carbonates, and the matrix of the meteorite. In total, over 40 imaging scans and 100 spot spectra were obtained. Approximately 30 globules were analyzed from within cracks and sealed inclusions in the BVC peridotites.

Optical and Scanning Electron Microscopy

Optical imaging was performed with an Olympus BX61 microscope coupled to computer control using Olympus Microsuite software. These images were then used to define areas of interest for Raman microscopy. To accurately determine the surface topography of fresh fracture faces and depths of areas of interest within thin sections for Raman measurements, 3-D extended focal imaging, using motorized z-control, was performed on globules and carbonates in ALH 84001 at 100×, 400×, and 1000×. In some cases, these measurements resulted in over 100 separate images being collated to produce a single, in-focus image and associated 3-D surface model.

After Raman microscopy, selected samples of interest were prepared for scanning electron microscopy (SEM) and energy dispersive X-ray analysis (EDX). Analysis and mapping were conducted using a JOEL 6500 field emission gun system with an associated Link Genesis EDAX system. Typically, an acceleration voltage of 15 kV was used on samples that had been mounted on carbon tape and gold/palladium coated for 30 s.

Raman Spectroscopy of Standard Materials

Raman spot spectra were collected for a number of known compounds to assist in assignment of the Raman bands observed in ALH 84001 and BVC carbonates. These standards were: calcite and magnesite obtained from in-house mineral collections; siderite provided by Bevan French (Smithsonian Institution); carbonaceous interplanetary dust (IDP) material, by Larry Nittler (Carnegie Institution); Gunflint microfossils, by Ed Vicenzi (Smithsonian Institution). Carbon glass and graphite were purchased from Sigma Aldrich. Further standard spectra of rutile and glass were obtained from the papers of Wang et al. (2004a, 2004b) and Cooney et al. (1999), as well as Raman databases provided by Washington University, Saint Louis, Missouri, USA; California Institute of Technology; and the University of Parma, Italy. In the case of BVC thin sections, reference spectra of the mounting and polishing polymers used to prepare the sections was also undertaken. A number of single spectra were obtained for all of these reference materials with similar acquisition times to those used in the study.

Raman Heating Study

Laser heating is known to transform carbonates (Cooney 1999). Therefore, to ensure that the laser power used was not affecting the samples, a study to incrementally increase the laser power during analysis was conducted. Single spectra at the lowest laser power (0.1 mW for 1 s) were obtained on freshly revealed surfaces of ALH 84001 globules. Laser power and integration times were slowly increased from 0.1, 0.5, 1, 5, and 10 mW for 1 and 5 s. After each spectrum was collected, the sample was inspected for signs of visible damage and the spectra compared for peak shift and changes in peak position. All power settings were measured at the objective. The experiment was also conducted on the siderite reference material to ensure that laser heating was not responsible for the observations of hematite in the ALH 84001 carbonates.

RESULTS

Optical Microscopy

All samples of ALH 84001 contained numerous carbonate globules (Figs. 1a–e; also Mittlefehldt 1994). Whereas some globules contained a white magnesite zone between two outer rims of magnetite—as identified from previous observations (McKay et al. 1996) and during Raman mapping—most had only a single magnetite rim (Figs. 1a and 1d). Dark- to light- colored orange carbonates were also present as chaotically diffuse patches, which occasionally overlapped with carbonate globules (Fig. 1b). We interpret these as the “slab carbonate” eluded to by Eiler et al. (1998) and Corrigan and Harvey (2004). Rings of magnetite without associated carbonate were observed throughout all allocations of ALH 84001. In some instances, carbonate was present in these features as a thin coating or isolated islands within the outer magnetite rim. The distribution of these magnetite rings appeared random, and in some places were within microns of carbonate-containing globules (Fig. 1a).

Magnetite, confirmed by Raman spectroscopy, was also observed as undulating threads passing through areas of diffuse, nonglobular carbonates or as small groups of crystals throughout the matrix of the meteorite. These patches of magnetite varied in size from submicron to >10 μm (Fig. 1a; also refer to Fig. 8a). In rare instances, fractured carbonate globules were observed with the golden-to-orange surface coloration not extending deeper than 1–2 μm into the surface, which were on average 4–6 μm thick (Fig. 1d). Abrading the surface of globules from ALH 84001 with a cleaned stainless steel needle showed a transition from the orange carbonate at the surface to a white carbonate beneath. This white carbonate contained small veins and concentrations of a reddish material (Fig. 1). In comparison, the BVC xenolith carbonates were predominately white throughout with darkened centers and rims.

Raman Spectroscopy

Reference spectra for hematite, magnetite, siderite, calcite, and magnesite were measured and compared to averaged spectra from ALH 84001 and BVC carbonates (Fig. 2). Designations ALH 84001-A, ALH 84001-D, and BVC 2 are explained below and are generated from analysis

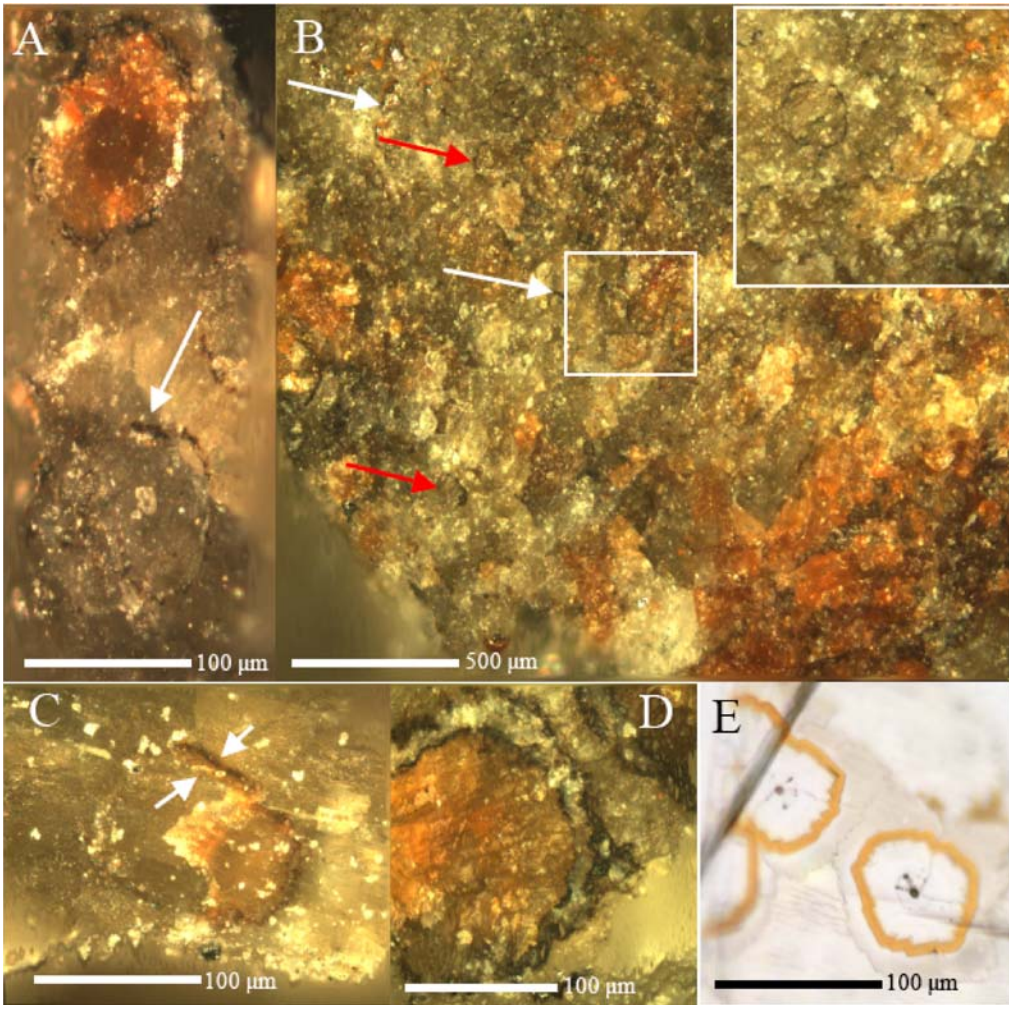

Fig. 1. Visible light microscopy and 3-D extended focal imaging of a range features from ALH 84001 and BVC xenoliths. a) A single globule from ALH 84001 336 with a dark center and a ring of magnetite surrounding it above a ring of magnetite with no internal carbonate (white arrow). b) An area containing slab carbonates, some with magnetite rims forming distinct globules, most diffuse with no obvious rims. Magnetite can also be seen as rings similar to that seen in Fig. 1a (red arrows) and meandering black lines and assemblages across the surface (white arrows). The insert shows a magnified image of the area indicated by the white box and shows a row of three magnetite rings (ALH 84001 332). c) A 3-D image of a broken carbonate globule revealing areas where the rim is intact in only half the globule. The impression of the rest of the carbonate globule is left behind and exposes the pyroxene beneath. The vertical distance between the two white arrows is ~5 µm (ALH 84001 347). d) A 3-D automontaged image of a single classically zoned carbonate globule from the center of ALH 84001 347. e) A number of globules contained on a fracture face of an olivine crystal from a BVC peridotite (transmitted light). Scale bars = 100 µm in (a), (c), and (d), 500 µm in (b), and 100 µm in (e).

shown in Fig. 3. The averaged spectrum from ALH 84001-A shows a peak distribution that is similar to that expected from a mixture of sideritic carbonate and hematite (see Table 1 for summary).

The carbonate intensity map at ~1090 cm^{-1} for globules from ALH 84001 and BVC did not reveal any information on the zoning of the globules in either sample's carbonates (Figs. 3a and 3d). Mapping the peak center shift of both the ~300 cm^{-1} and ~1090 cm^{-1} peaks did, however, reveal chemical zoning of the globules carbonates (Figs. 3b and 3d). From Raman spectra of the carbonate standards, the peak center distribution of both the ~300 and ~1090 cm^{-1} bands of ALH 84001 and BVC carbonates indicates four distinct zones in ALH 84001 (labeled a–d in Figs. 3b and 3d). There are only two zones measured in the BVC carbonates (labeled 1 and 2 in Figs. 3b and 3d).

A trend of the ~300 cm^{-1} band to higher wavenumbers indicates increasing Mg-rich carbonate. Decreasing frequency indicates compositional changes toward siderite and calcite (Fig. 3f). Comparing the trends of the standards and the ALH 84001 and BVC carbonates reveals a progressive trend from a more calcite- and siderite-rich carbonate (probably ankerite) near the center to siderite/magnesite-rich carbonate at the outer rim (Fig. 3f). This is consistent with previous observations (McKay et al. 1996 and references therein). The composition of carbonate from

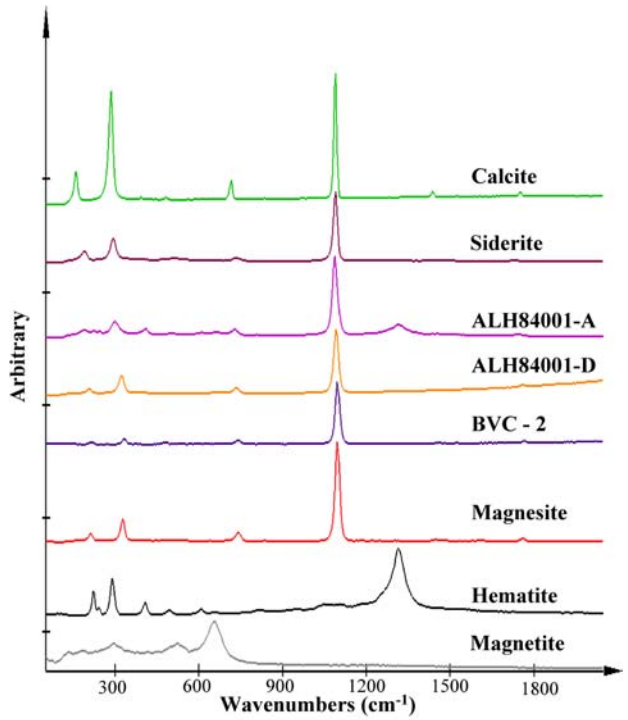

Fig. 2. Reference Raman spectra of calcite, siderite, magnesite, magnetite, and hematite together with representative spectra from ALH 84001 and BVC carbonate. ALH 84001-1 is an average spectrum from the center of an ALH 84001 globule (zone a as shown in Fig. 3b); ALH 84001-2 is an averaged spectrum from zone d in Fig. 3b.

zone 1 of BVC carbonates closely matches that of zone D in the ALH 84001 carbonates. Zone 2 of the BVC samples is almost pure magnesite and appears marginally less iron-rich than the magnesium carbonates from the outer rims of ALH 84001 (ALH 84001-D).

Three carbonate globules contained within an interstitial pocket of a BVC spinel lherzolite xenolith were imaged with light microscopy and the Raman microprobe (Fig. 4). The center is comprised of carbonate, hematite, and magnetite with an adjacent magnesite-rich carbonate layer, which in turn is bounded by an outer rim of hematite, magnetite, and magnesite. Carbon was identified by characteristic bands at ~1350 (D band) and 1610 cm^{-1} (G band) (Pasteris and Wopenka 2003). The carbon spectra were indicative of mainly amorphous macromolecular material (Fig. 5) that was found spatially associated with rings of magnetite at both the center and periphery of the globule. These globules are representative (~15 from 30 imaged) of a distinct class of magnetite and MMC containing globules within the BVC xenoliths. MMC was not associated with hematite. Figure 5 shows spectra of MMC found in BVC carbonates and ALH 84001 compared to that of MMC spectra from samples of crystalline graphite, carbon glass, terrestrial fossiliferous kerogen, and an interplanetary dust particle (IDP). All types of MMC analyzed displayed characteristic D and G band

Table 1. Peak assignments for siderite, hematite, and a representative average of the core of ALH 84001. Peak intensity is represented in the following manner: vw = very weak; w = weak; m = medium; ms = medium strong; s = strong; and vs = very strong.

Siderite	Hematite	ALH 84001 core
189 m		187 m
	221 ms	223 w
		241 w
292 s	287 ms	296 ms
	406 m	406 ms
	491 w	492 w
	607 w	609 w
	655 w	655 vw
731 s		726 m
	955 w	
	1049 w	
1088 vs		1085 vs
	1115 w	
	1314 vs	1314 vs
1734 w		1744 w

peaks at ~1350 and ~1600 cm^{-1}, respectively. The majority of carbon found in BVC and ALH 84001 samples (BVC and spectra ALH 84001-2) displayed very broad D and G bands similar to the carbon spectra of IDPs and kerogen. The spectra of BVC carbonate and the IDP are from single spot spectra and show weak but definite carbon peaks. The second order Raman band of carbon (2700–3000 cm^{-1}) was present in the graphite, carbon glass, and ALH 84001-1 spectra. Kerogen from the gunflint fossil showed a broad increase in the background from 2600–3000 cm^{-1}, but no specific peaks were observed. No other samples contained evidence of a distinctive second order peak. ALH 84001-1 had narrower D and G peak widths than the ALH 84001-2 spectra, which is similar to those seen in carbon glass and graphite. Coupling this observation with the presence of a second order carbon peak appears to confirm that the MMC in ALH 84001-1 is more graphitic in nature than that in ALH 84001-2, thus illustrating there is a range of MMC in ALH 84001 tending from very amorphous to more graphitic.

A trio of globule assemblages on a fracture surface of ALH 84001-357 was mapped to determine the distribution of characteristic spectral peaks (Fig. 6a). In Figs. 6b–g, individual spectral maps show the distribution of carbonate, pyrrhotite, magnetite, hematite, and MMC. Whereas hematite and pyrrhotite were distributed heterogeneously throughout the globules, magnetite was concentrated mostly within the rims and as discrete 0.5–5 μm patches within the carbonate globules. The optical and Raman images from another globule of the same sample are shown in Figs. 6g–j. MMC, where present (Fig. 6h), appeared as discrete small domains within the magnetite rims. Figure 6k shows the transition between sideritic carbonate (dark brown) to magnesitic carbonate (yellow) across the magnetite rim (Fig. 6i). This trend is further illustrated in Fig. 6l, which is a histogram of peak centers from the same area as Fig. 6f, and shows a

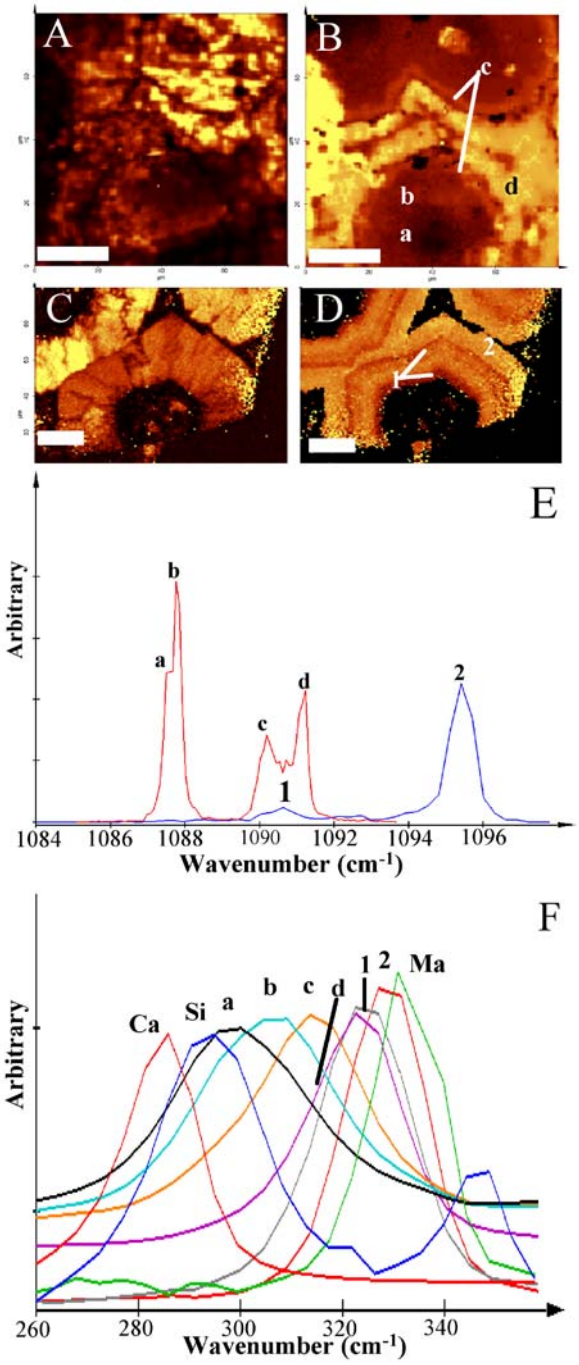

Fig. 3. a) The carbonate distribution (~330 cm^{-1} carbonate peak) across an area of three carbonate globules contained in ALH 84001-357. b) The peak center shift of the carbonate 330 cm^{-1} peak showing four distinct zones, marked by the letters a–d. The lighter colors show a peak shift toward higher wavenumbers. The bright yellow areas are an artifact of fluorescence. c) Same peak distribution as (b), from a BVC carbonate assemblage. d) The peak center shift of the carbonate 330 cm^{-1} peak showing a more complex zoning pattern than that seen in (b). The marked areas 1 and 2 are used to delineate the light and dark areas in the zoning pattern. In (a) and (c), the lighter coloration indicates a more intense peak signal. In (b) and (d), the lighter coloration indicates a peak shift toward higher wavenumbers. e) The peak center distribution histogram of the carbonate 1090 cm^{-1} peak for the carbonates shown in (a) and (c). ALH 84001 is shown in red and exhibits four distinct peaks indicative of the zones seen in (b); BVC is in blue and shows two distinct peaks correlating to the areas marked in (d). f) The 260–360 cm^{-1} area of nine spectra (numbers in brackets indicate number of spectra averaged). Ca = calcite standard (25); Si = siderite standard (25); a = averaged spectra of zone a of ALH 84001 from (b) (~500); b = averaged spectra of zone b of ALH 84001 from (b) (~800); C = averaged spectra of zone c of ALH 84001 from (b) (~160); d = averaged spectra of zone d of ALH 84001 from (b) (~250); 1 = average spectra from zone 1 of BVC carbonate as shown in (d) (~120); 2 = average spectra from zone 2 of BVC carbonate as shown in (d) (~180); Ma = magnesite standard (25).

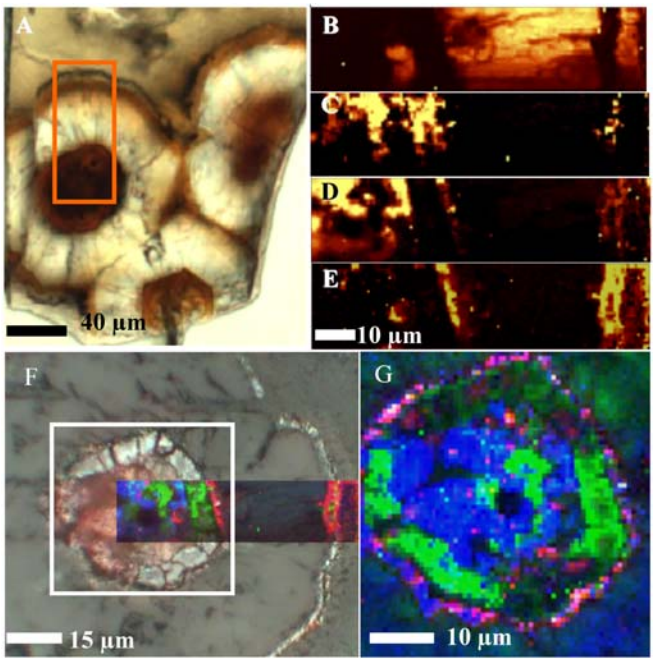

Fig. 4. a) Light microscopy imaging of three BVC carbonate globule within an olivine grain of a BVC mantle xenolith. The orange box indicates the area mapped in Fig. 4b–e rotated 90° clockwise. b) Peak map of the occurrence of the carbonate ~1090 cm^{-1} peak. c) Peak map of the hematite ~295 cm^{-1} peak. d) Peak map of the magnetite ~670 cm^{-1} peak. e) Peak map of the carbon G band peak at ~1600 cm^{-1}. f) Reflected light microscopy image of the globule marked by the orange box in Fig. 4b. Overlaid on this image is a compilation Red Green Blue (RGB) image of the peak maps of hematite (green), magnetite (blue) and carbon (red). g) A RGB compilation of the center of the globule marked by the white square in Fig. 4f. Green is hematite, blue magnetite and red carbon (using the same peak assignments as outlined in Fig. 4c–e). The purple/pink coloration is caused by the exact overlay of magnetite (blue) and carbon (red).

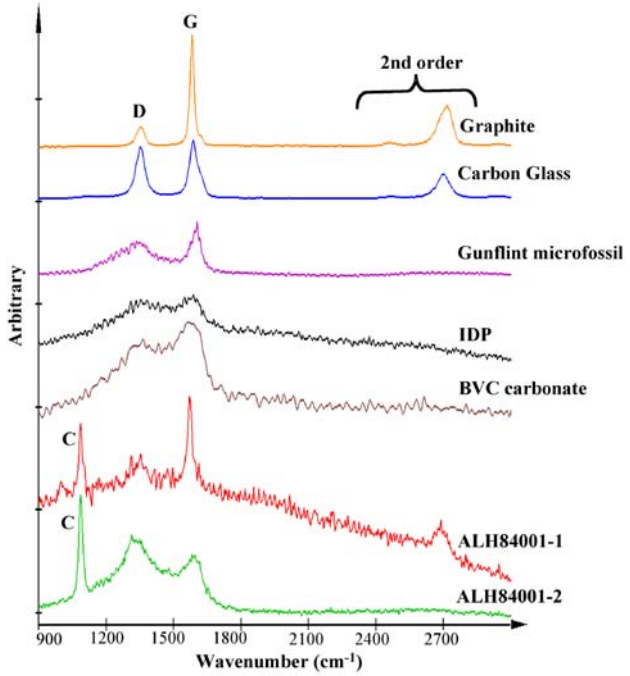

Fig. 5. Spectra of graphite and macromolecular carbon from a range of samples including graphite, carbon glass, a single gunflint microfossil, an IDP, BVC carbonate, and two spectra representative of the spread of carbon spectra in ALH 84001. D = disordered Raman band of carbon at ~1350 cm^{-1}; G = ordered (or graphitic) band of carbon at ~1570–1610 cm^{-1}; 2nd order = the second order Raman bands at 2700–3000 cm^{-1}; C = carbonate 1090 cm^{-1} peak.

bimodal distribution with the peak centered at 303 cm^{-1} indicative of sideritic carbonate, and that at 317 cm^{-1} indicative of a more magnesitic carbonate.

Optical and Raman peak images of a diffuse (or slab) carbonate in ALH 84001-380 are shown in Figs. 7b–f. MMC was again associated with magnetite as in the other ALH 84001 samples. An area of slab carbonate was associated with a phase whose Raman spectra are suggestive of plagioclase composition glass (Figs. 7g, 7h, and 7i). In the detailed image in Fig. 7i, the areas of high carbonate abundance were deliberately over-emphasized to reveal the signal from a small concentration of carbonate layered over a plagioclase phase.

Throughout the matrix of every analyzed sample are numerous areas of irregular optically dark assemblages of magnetite (Fig. 8). These assemblages range from single crystals to larger, 10–50 µm aggregates of smaller crystals. MMC material is present in most of the analyzed assemblages. An irregular black deposit within the host pyroxene (Figs. 8a and 1b) of ALH 84001-347 contained significant patches of MMC associated with magnetite and in some cases hematite, rutile, and small mounts of sideritic-rich carbonate (Figs. 8b–e). Figure 8f is of the pyroxene host.

Analyses of both slab and globule core carbonates in ALH 84001 revealed the pervasive presence of hematite within the carbonate phase (Fig. 2; Table 1). A freshly abraded globule reveals that the orange coloration of the globules extends only a few micrometers into the surface, after which the carbonate appears white with a distinct pink to reddish cast. Raman peak images of the transition between orange and white/pink carbonate (Figs. 9c–f) show little variation in the hematite and carbonate distribution. The arrow in Fig. 9a highlights a small magnetite grain, associated with MMC from ALH 84001-347 (see arrows in Fig. 9e and 9f). Electron microscopic imaging of the carbonates reveals that the external surface (i.e., the orange color) of the carbonates has a different surface texture than that of the freshly revealed carbonate. The surface was covered with small pits and appeared more altered than the interior. The freshly revealed carbonate surface exhibits a cuboidal fracture texture and contains myriad small crystallites (~50 nm) that pervade the carbonate (Fig. 9h). Laser heating visibly damaged freshly revealed surfaces only after the laser power was increased above 10 mW, an intensity significantly greater

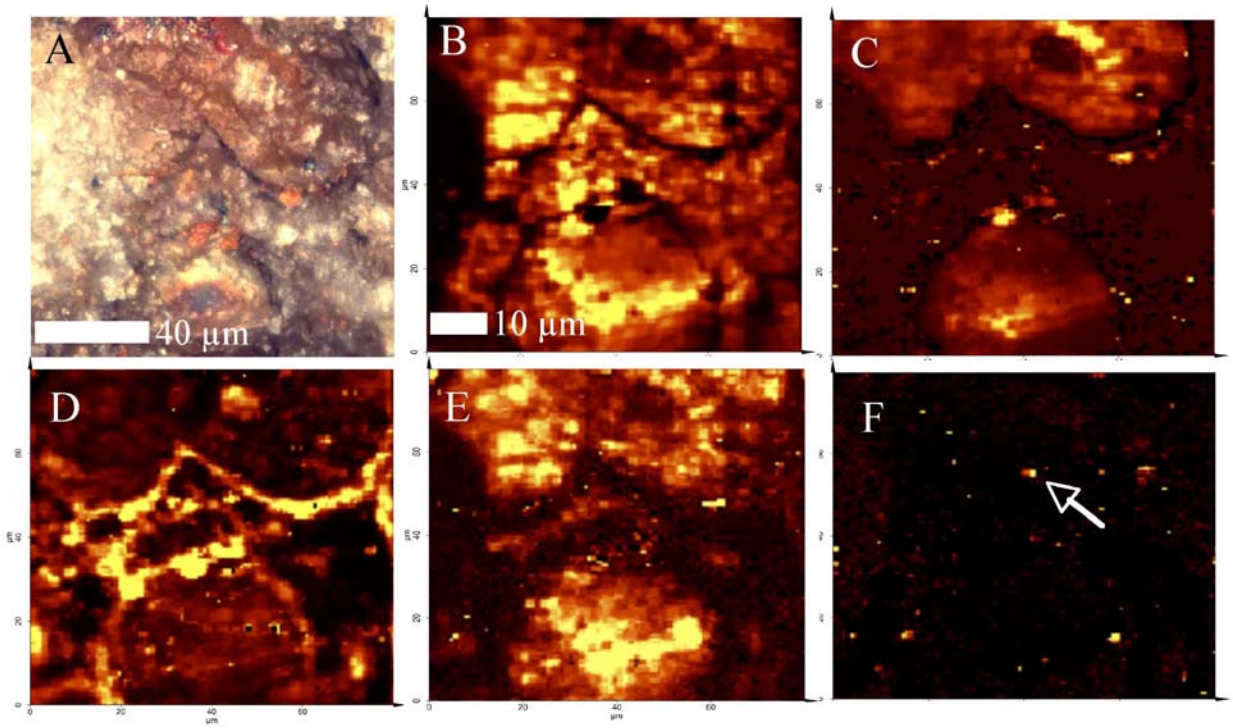

Fig. 6. a) Light microscopy Z stack montage of a trio of carbonate globules from ALH 84001-380. (b–f) are Raman peak maps (80 × 80 µm) of: b) carbonate (~1090 cm^{-1}) (note the lighter the color the more intense the signal); c) pyrrhotite (290 cm^{-1}); d) magnetite (665 cm^{-1}); e) hematite (~220 cm^{-1}); f) carbon G band (~1610 cm^{-1}).

than the 0.3–1 mW used in this study. The area shown in the white box in Fig. 9b was mapped before beginning the heating study at another position on the sample (white arrow in Fig. 9b). No visible damage to any surface or change in Raman spectra was observed using 0.3–1 mW and 5 s integration times. In fact, hematite was detectable at the lowest limit of laser power (0.1 mW) and an integration time of only 1 s.

DISCUSSION

Light Microscopy

Light microscopy (Fig. 1) confirmed previous suggestions as to the provenance of several types of carbonate in ALH 84001 (Eiler et al. 1998; Corrigan and Harvey 2004). The diffuse patches of carbonate imaged in this study are probably the diffuse patches or "slab" carbonates that have previously been described (Eiler et al. 1998; Corrigan and Harvey 2004). These carbonates are not globular in shape or bounded by magnetite and magnesite and represent a second morphology to the carbonate globules.

Both the ALH 84001 and BVC globules appear to be slightly recessed into the host mineral (seen in Fig. 1c). This suggests that some interaction between the host rock and the globules took place during their formation. Many surfaces contain rings of magnetite with little or no carbonate associated with them. We postulate that these rings once contained carbonates as it seems very unlikely for magnetite to spontaneously crystallize in such a fashion. Furthermore, some of these rings contain small pockets of carbonate associated with the magnetite. Therefore, if all of these magnetite rings once contained carbonate, we may evaluate two possible explanations: 1) the carbonate was dissolved or vaporized, or 2) it cracked and broke off during sample preparation. We discount scenario 2 because examination of numerous broken globules (as shown in Fig. 1c) revealed that carbonate and magnetite were both removed when the globules fractured. Brearley (2003) points out that the outer magnetite rims of carbonate globules appear fractured in their contact with the surrounding matrix, therefore predisposing both the carbonate and rims to be removed during any mechanical stress on the globules. Secondly, there are no carbonate rings without an outer magnetite ring, as may be expected if the carbonate was left behind on an opposing crack surface during splitting of the meteorite. We are, therefore, left with the observation that the siderite originally contained in these magnetite rings was removed by either dissolution or vaporization.

Raman Analysis of Carbonates

Carbonate globules in ALH 84001 show a progression from a calcium-rich siderite, probably ankerite core to

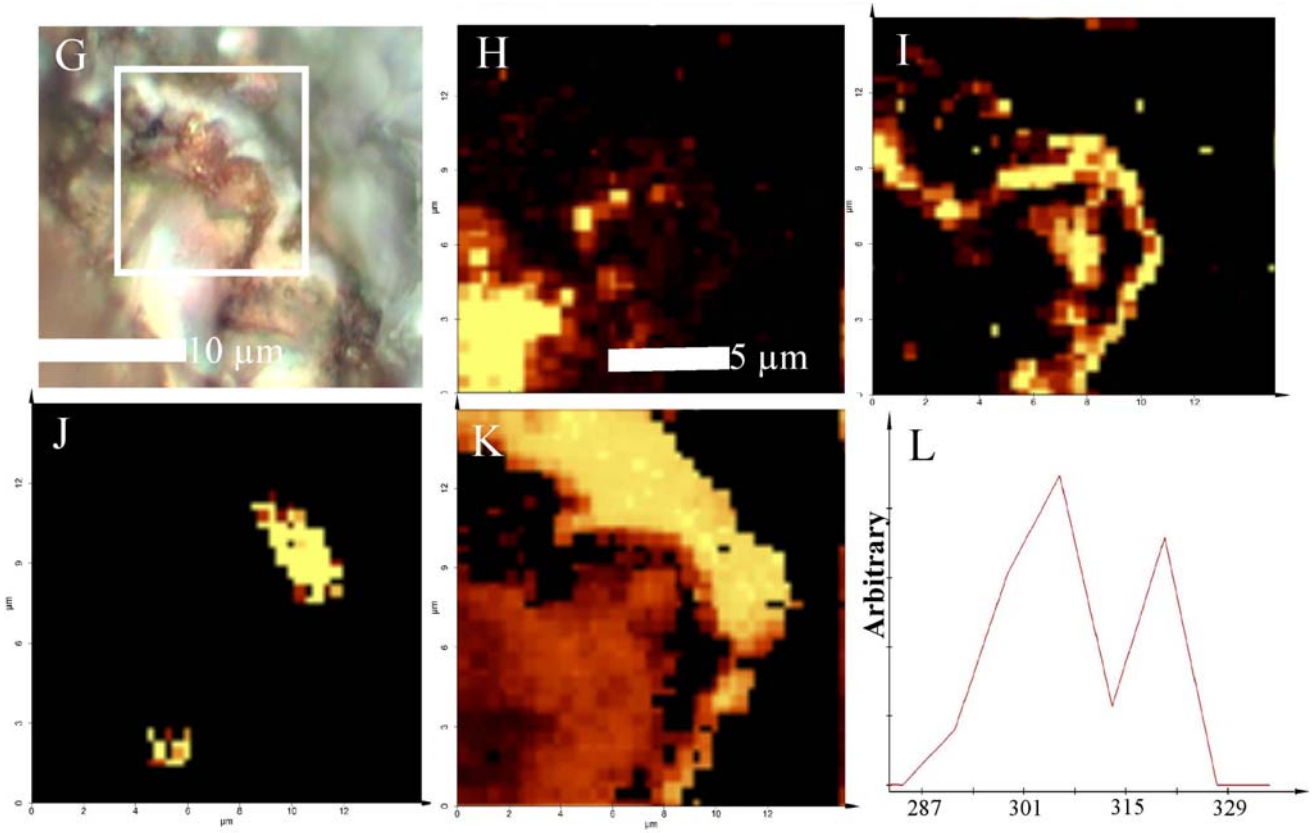

Fig. 6. *Continued.* g) Light microscopy image of the rim of a single carbonate globule from ALH 84001-357. The white box denotes the area of peak mapping in the Raman investigation shown in (h–k). h) Hematite (~220 cm^{-1}). i) Magnetite (665 cm^{-1}). j) Carbon G band (~1600 cm^{-1}). k) Carbonate ~300 cm^{-1} peak center map. Lighter colors show a shift to higher wavenumbers. l) Peak center distribution histogram of the carbonate ~300 cm^{-1} peak showing the bimodal distribution visualized in (k).

magnesian carbonate at the rim. Calcium has been detected by elemental analysis in the core (McKay et al. 1996). However the characteristic ~180 cm^{-1} peak of calcite was not detected in this study, suggesting that the calcium is present within a sideritic carbonate, possibly as ankerite. This observation correlates with previous studies (Mittlefehldt 1994a, 1994b, 1997; McKay et al. 1996). Carbonate Raman spectra exhibit a peak near ~ 300 cm^{-1}, which is assigned to a librational lattice mode. The position of this peak is sensitive to the composition of the carbonate such that the peak generally shifts to higher wavenumbers as larger mass cations are incorporated (Clooney et al. 1999). The BVC globules vary from an iron-rich magnesite in the core to almost pure magnesite at the rim. The zoning pattern in BVC globules, however, is spatially much finer than in ALH 84001, and oscillates between these two end members before magnetite deposition begins at the outer rim. The wide range of carbonate chemistry in ALH 84001, along with oxygen isotope measurements, has been used to infer a multiple depositional origin for the carbonate globules (Saxton et al. 1998). Conversely, the BVC globule samples are known to have formed from a single event during the time of the eruption of Sverrefjell volcano about 1 Myr ago. BVC carbonate chemistry (Fig. 3) varies as widely as in ALH 84001, thus indicating that the zonation seen in ALH 84001 could occur during primary formation of carbonate globules. Complex zonation is also seen in these "slab carbonates" that is similar to variation observed proximal to magnetite in the globules. Corrigan and Harvey (2004) discuss the formation of these carbonates as a single event, which adds weight to the argument that the globules in ALH 84001 also formed from a single event.

The association of plagioclase-like glass with slab carbonate has been observed in two areas analyzed in this study. We find no evidence that the glass intruded through an established carbonate assemblage. Rather, a thin film of carbonate was layered over the glass, revealing that carbonate deposition post-dates glass formation, which is in general agreement with the observations of Corrigan and Harvey (2004).

Macromolecular Carbon (MMC) and Magnetite

In many of the ALH 84001 globules, MMC is associated with magnetite both in the rims (Figs. 6f and 6j) and around small magnetite particles inside fresh internal carbonate surfaces (Fig. 9f). MMC also occurs in the magnetite

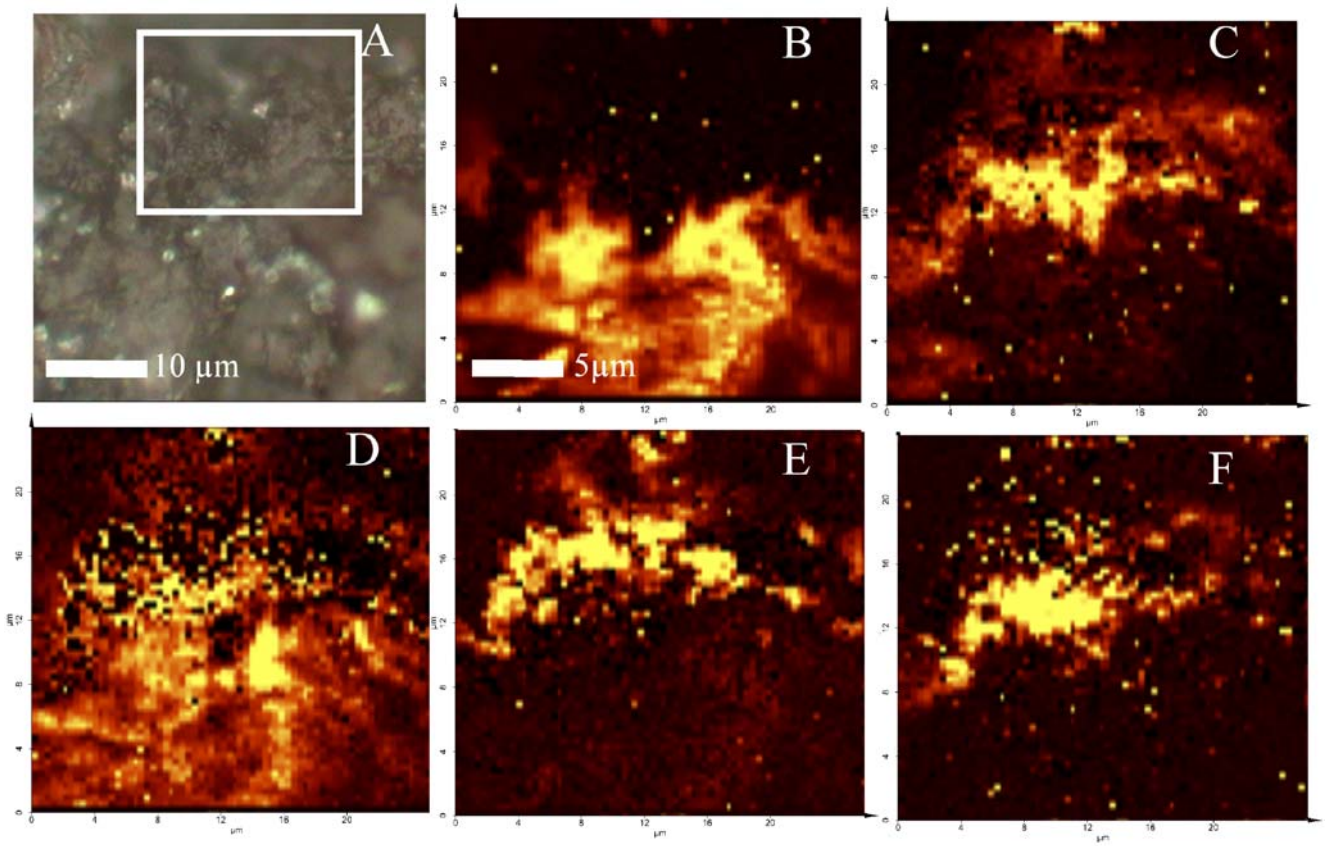

Fig. 7. Visible light and Raman peak maps of slab carbonates from ALH 84001 380 (box in [a] and [b–f] are 24 × 24 µm) of a carbonate magnetite assemblage. The lighter color indicates a more intense peak). a) Light microscopy image with the white box showing the scan area. b–f) Raman peak maps of: b) Carbonate (~1090 cm^{-1}). c) Magnetite (~665 cm^{-1}). d) Hematite (~220 cm^{-1}). e) Pyrrhotite (~290 cm^{-1}). f) Carbon G band (~1600 cm^{-1}). g) An area of slab carbonate from the same sample overlaying an area of plagioclase. (h–l) are Raman peak maps for: h) Plagioclase (~500 cm^{-1}). i) Carbonate (~1090 cm^{-1}). j) Hematite (~220 cm^{-1}). k) Magnetite (~665 cm^{-1}). l) Carbon G band (~1600 cm^{-1}). The last two images have been processed to remove areas of background fluorescence.

associated with slab carbonates, either as individual grains or clusters (Fig. 7), or with irregularly sized areas of magnetite throughout crack surfaces (Fig. 8). Out of twenty globules imaged throughout the depth profile, five showed patches and/or bands of MMC from areas within the rims. Eight globules have small patches of MMC within the inner sideritic zones of the carbonate globules where they are always associated with small regions of magnetite. Out of eight areas of magnetite analyzed in the matrix, seven contain evidence of MMC (Fig. 8).

MMC in ALH 84001 varies from very ordered (very graphitic) to very disordered (similar to IDPs) (see Fig. 5). The vast majority of MMC found in ALH 84001 is relatively amorphous, with crystalline graphite occurring in two localities among the matrix magnetite assemblages analyzed. Indigenous MMC, which may include PAHs, has been found within ALH 84001 (Becker et al. 1999; Clemett et al. 1998; Jull et al. 1998; McKay et al. 1996). PAHs have also been detected in the MMC/graphitic component of carbonaceous chondrites and IDPs using the same techniques as applied to ALH 84001 by the McKay et al. team, i.e., two-step laser ablation mass spectrometry (Messenger 1998; Clemett and Zare 1997). Raman spectroscopic analyses of similar material (i.e., carbonaceous chondrites and IDPs) show a peak distribution of MMC similar to that found in this study (Fig. 4) (for examples, see Nakamura et al. 2002). We conclude, therefore, that the PAHs originally found in ALH 84001 by McKay et al. (1996) are related to the pool of carbon analyzed in this study.

Graphite has been previously detected by Raman spectroscopy in the Martian meteorite NWA 1068 (Hochleitner 2004). The Raman peak distribution in ALH 84001 shows broad peaks at both ~1600 and 1350 cm^{-1} (G and D band) that are indicative of MMC and not of poorly ordered or crystalline graphite (Fig. 5). While Pasteris and Wopenka (2003) have shown that this peak distribution does not indicate a biological or abiological origin for MMC, however, the peak distribution of graphite and poorly ordered graphite are significantly different from kerogen or MMC (Fig. 5). Therefore, to reiterate, the D and G bands of carbon Raman spectra cannot discriminate between known biological signal (Gunflint microfossil) and the nonbiological carbon in IDPs.

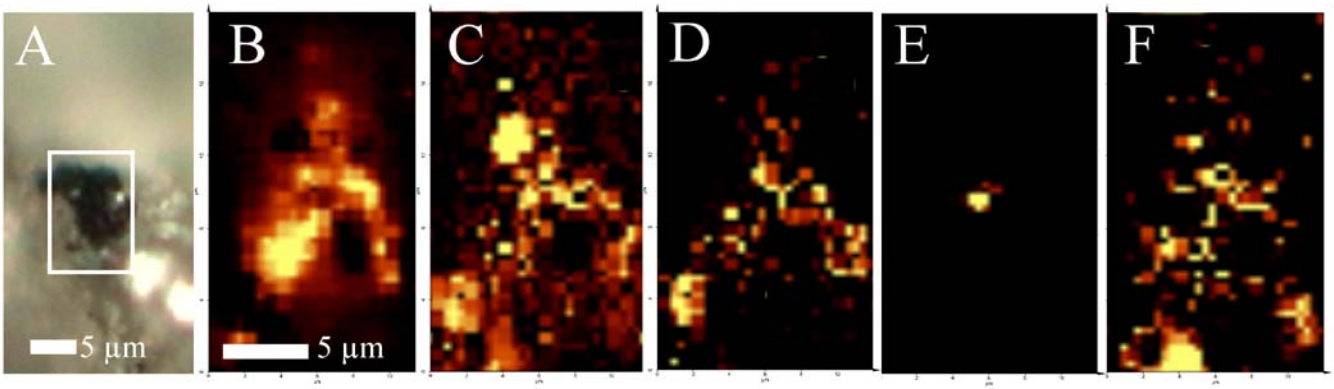

Fig. 8. a) Visible light microscopy of black crystalline feature occurring in the matrix. (b–f) represent Raman images of a 12 × 20 µm area of the black area shown in (a). Higher signal intensity is shown by lighter colors. b) Carbon (G band at ~1600 cm^{-1}). c) Magnetite (~665 cm^{-1}). d) Hematite (~220 cm^{-1}). e) Rutile (~420 cm^{-1}). f) Pyroxene (~1005 cm^{-1}).

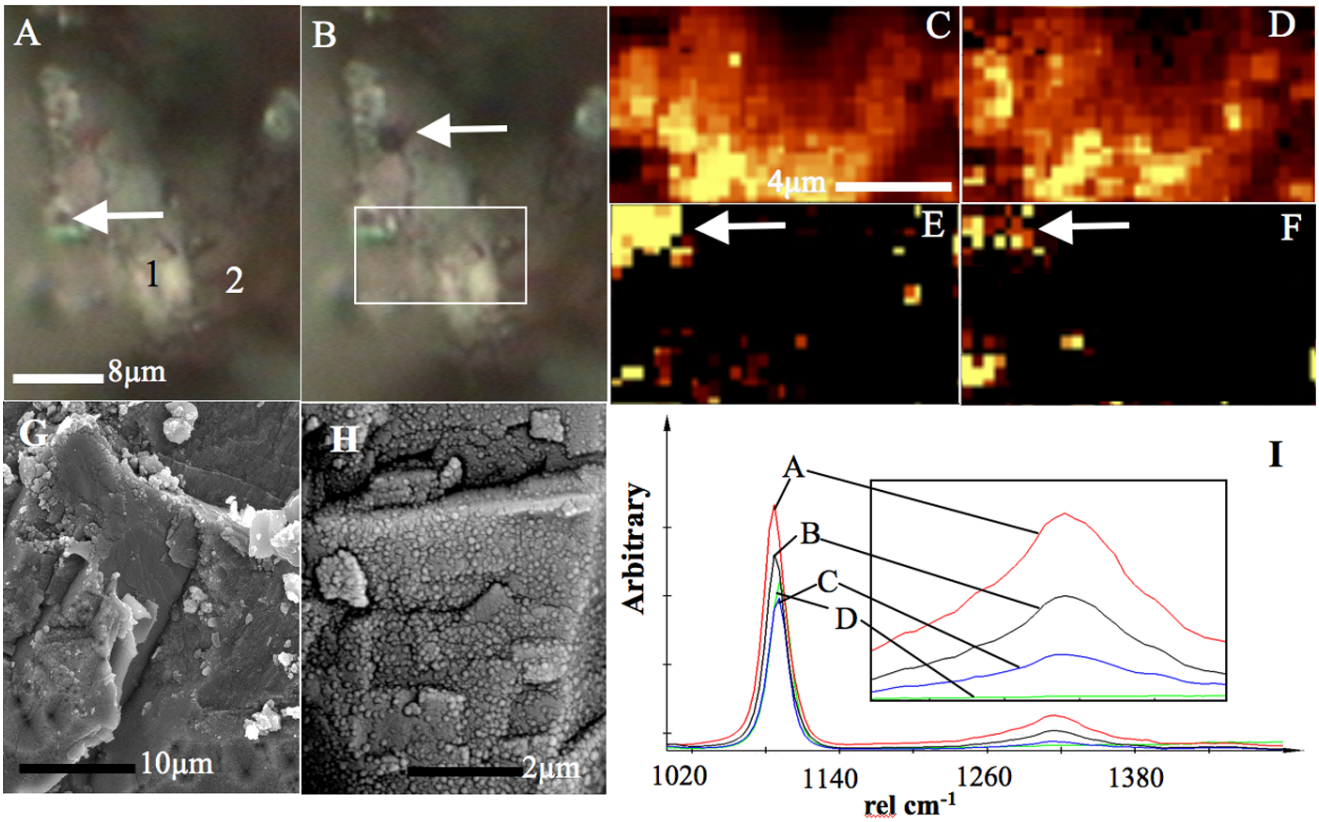

Fig. 9 a) Light microscopy image of a freshly scratched globule (from Fig. 1b ALH 84001-347). Area 1 shows a white area with an overall pink to red cast; area 2 shows the typical orange color of the outside layer of the globule. The arrow shows a small magnetite assemblage (e). b) The same area but after analysis with a 20 mW laser beam; the arrow points to the damaged area. The white box indicates the area scanned during Raman peak mapping shown in (c–f). Note this area was scanned before the heating experiment, which produced the alteration seen in (b). c) Carbonate (~1090 cm^{-1}). d) Hematite (~220 cm^{-1}). e) Magnetite (~665 cm^{-1}). f) Carbon G band (~1600 cm^{-1}). Arrows in (e) and (f) show black area marked by an area in (a). g) A secondary electron image of the scratch (lower right of white box in [b]) showing different carbonate morphologies from an outer pitted texture (lower part of image), to successively deeper layers with no pitting and layering (top right of image). h) High-magnification image of the white-pink area revealed by scratching the globules shows apparent numerous nanocrystallites in the carbonate. i) A qualitative comparison of the intensity of the hematite (~1310 cm^{-1}) peak for ALH 84001 zones a–d, as illustrated in (b). While for ease of viewing the peaks in this image are not normalized to the carbonate peak intensity, normalizing does not effect the distribution seen in the insert, which shows a progressive decrease in hematite peak intensity from zones a–d.

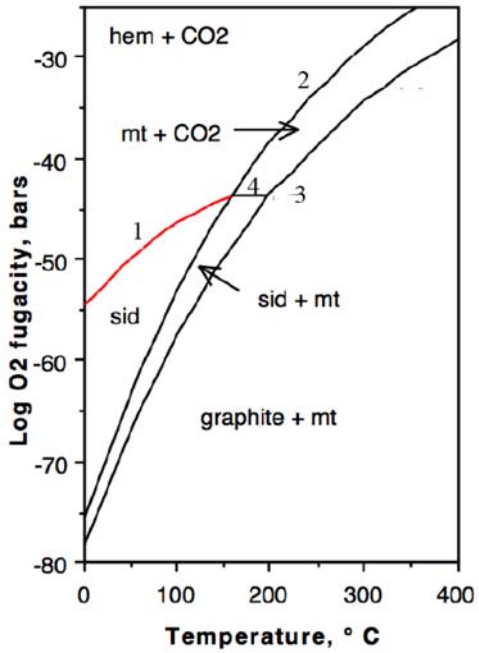

Fig. 10. The stability fields of hematite, magnetite, siderite, and graphite at 1 bar CO_2 pressure over range of temperatures and oxygen fugacities, reproduced with kind permission from Koziol (2000). Curves are constrained by the following reactions: 1) $2FeCO_3 + 1/2O_2 = Fe_2O_3 + 2CO_2$; 2) $2Fe_3O_4 + 1/2O_2 = 3Fe_2O_3$; 3) $3FeCO_3 = Fe_3O_4 + 3C_{(graph)} + 5/2O_2$; and 4) $3FeCO_3 = Fe_3O_4 + 2CO_2 + CO$. mt = magnetite; sid = siderite; and hem = hematite. The curve bound by reaction 2 is that of the hematite magnetite buffer.

We conclude that the carbonaceous material detected in our study is composed of MMC containing a range of compounds including polyaromatic species, and that the D and G band Raman peak distribution of MMC is similar to that found in carbonaceous chondrites and IDPs. Becker et al. (1999) demonstrated the presence of MMC in the matrix of ALH 84001. Flynn et al. (1999 and 2000) showed the presence of C-C, C=C, and possibly C-H bonds in both carbonate and rim material (Becker et al. 1999; Flynn et al. 1998; Flynn et al. 1997).

The presence of MMC within carbonate globules in lherzolite xenoliths from BVC suggests that macromolecular carbonaceous material can be generated during carbonate deposition within mantle rocks on Earth. Thermodynamic calculations and experimental data on the thermal breakdown of siderite show that PAHs, graphite, and MMC are produced and this observation has been used previously to explain the presence of PAHs in ALH 84001 (Koziol 2001, 2004; McCollom 2003; Treiman 2003; Treiman et al. 2002; Zolotov and Shock 2000). Although a thermal decomposition of siderite origin for PAHs in ALH 84001 is possible and indeed may have played a role, the studies on BVC show that magnetite and carbonates associated with MMC can form during primary development of the globules.

An explanation of the development of BVC and ALH 84001 carbonate assemblages requires an understanding of the phase relationships of iron oxides, graphite, and CO_2 (Fig. 10, reproduced with kind permission from Koziol 2001) over a range of pressure, temperature and oxygen fugacities (French 1971, 1965; Koziol 2004, 2000; Weidner 1972). The stability field for siderite is small in temperature/fO_2 space compared to that for magnetite and graphite. Therefore, during formation of both the BVC and ALH 84001 globules, large fluctuations in oxygen fugacity (up to ~–40 log units of fO_2) and temperature were possible. However, as the temperature decreases from 400 °C to 0 °C, so does fO_2 in a system buffered by hematite and magnetite. This is not an unreasonable assumption given the presence of both hematite and magnetite in BVC and ALH 84001 (Koziol 2004). For BVC globules, this situation is rational given the fact that after ejection from Sverrefjell, the BVC xenoliths were exposed to arctic temperatures. Hot CO_2-containing aqueous fluids cooled rapidly, during which time the oxygen fugacity fell, thus promoting the formation of reduced-carbon phases alongside magnetite. During this process, the conditions in BVC samples evidently entered the magnetite/graphite stability field twice, as MMC carbon with magnetite is detected in both the center and the outer rims of the carbonate globules. While the stability field that includes reduced carbon technically describes the carbon as graphite, the low temperatures and corresponding lack of kinetic energy for crystalline graphite formation should reasonably produce the MMC and PAHs found in this study and others. It has also been noted that the formation of MMC and PAHs is energetically favorable even at moderately high H_2 fugacities (Eck 1966; Zolotov and Shock 2000). Hydrogen would be present in this system from dissociation of water and perhaps linked to dissolution of the host mineral matrix (Fig. 1c). These conditions would all predispose the formation of MMC observed in both BVC carbonates and ALH 84001. Similar interaction between CO_2 and FeO have also been proposed as being responsible for MMC reservoirs in meteorites and IDPs, although it has not previously been confirmed as a process in Martian samples or indeed terrestrial mantle rocks (Allamandola et al. 1988; Anders 1991; Anders et al. 1996; Nakamura et al. 2002; Wopenka and Swan 1985).

To Heat or Not to Heat?

ALH 84001 has undergone a complicated heating history compared to the BVC carbonates, which makes interpreting the mechanism of MMC formation in ALH 84001 complicated. Debate is continuing as to whether a shock heating event occurred after carbonate globule formation and its subsequent effects on the carbonate globules (Bell and McKay 2000; Brearley 2003; Eiler et al. 2002; Scott et al. 1998a, 1998b; Scott et al. 1997a, 1997b; Treiman 1995, 1998a, 2003). Evidence from the interactions of carbonate

with plagioclase composition glass, the formation of voids around magnetite within slab carbonates and other petrographic studies are thought to constrain a high-temperature impact event (Bell and McKay 2000; Brearley 2003; Eiler et al. 2002; Scott et al. 1998a, 1998b; Scott et al. 1997a, 1997b; Treiman 1995, 1998a, 2003). One event, known as the I3 shock event, would have produced a heat pulse between 200 and 450 °C with pressures of up to 50 GPa, which should decompose siderite to magnetite and CO_2, as well as produce the observed PAHs (Treiman 2003). Evidence from remnant magnetism in the magnetite and pyrrhotite of the globules, combined with petrographic studies of plagioclase grains, however, indicates that this meteorite has not been exposed to a temperature above 40 °C or a change in bulk rock temperature of more than 120 °C (Fritz et al. 2005; Weiss et al. 2000; Weiss et al. 2002). In their paper, Fritz et al. (2005) do not preclude localized temperature spikes or transient events throughout the existing cracks in the rock. Therefore the observed petrography may only reflect the last impact event, as previous impact event textures would be reset (Fritz 2006, personal communication).

It has also been suggested that the outer rim of dual rim globules was formed by thermal decomposition of siderite during a shock event to leave magnesite and magnetite (Barber and Scott 2003; Barber et al. 2001; Scott et al. 2002; Scott et al. 1998; Treiman 2003; Golden et al. 2001). Brearley (2003) speculated that fracturing of the magnetite rim matrix boundary is evidence of a volume decrease associated with magnetite formation from siderite during a shock event. Concomitant to the shock event, Brearley (2003) proposed that during this heating event, the meteorite was experiencing considerable thermal heterogeneity, a factor expanded upon by Treiman (2003). This possibly explains the observations of Corrigan and Harvey (2004) that high-temperature interactions between carbonate and glass were not apparent in the samples they studied, as opposed to other studies (e.g., Barber and Scott 2003). However, Brearley (2003) based his speculation on voids around magnetite whose presence was due to formation of the magnetite from siderite. Based on the observation of MMC associated with magnetite within carbonates (Figs. 9e and 9f), another possibility is that this void space contained carbon removed during processing of the samples for TEM investigation, therefore questioning the interpretation of a shock formation mechanism for the magnetite in both the rims and within the globules.

Two types of carbonate globules (Fig. 1) have previously been described in ALH 84001: dark brown globules containing a single magnetite rim, and lighter orange-colored globules with a second magnetite outer rim bounded by an area of magnesite (e.g., Figs. 1a and 1d) (McKay et al. 1996; Treiman et al. 2003). To further hypothesize on the possible effects of heating on ALH 84001 globules, in this paper, we postulate the existence of a third type of globule. Type 1 are examples of globules (brownish with magnetite rims) that have not been heated to the point of decarbonation, although they would have experienced some transient heating event. Type 2 are examples of type 1 globules that have produced a secondary magnetite rim from iron-rich carbonate, which extended past the inner magnetite rim (the typical ALH 84001 globule). We do not know whether this is a primary depositional feature or one formed from a later shock event. Type 3 globules are rings of magnetite that are the remains of type 1 globules that have undergone decarbonation, probably during impact. The sulfur-containing mineral pyrrhotite found in the rims of globules (Figs. 6c and 7e) has also been suggested to form from decomposition of pyrite during a thermal event after primary precipitation, and thus both type 1 and 2 globules may have experienced some transient heating event (Golden et al. 2004a). The low temperature/pressure history for ALH 84001 after globule formation could possibly be resolved by magnetic measurements. Any secondary heating event above 40–80 °C (Weiss et al. 2000) should have destroyed the magnetic properties of primary deposited magnetites and pyrrhotites in all globule types, unless the magnetite and pyrrhotite in the outer rim of type 2 globules and the magnetite within the matrix were formed in this event. The conditions of the shock removal of ALH 84001 from Mars postulated by Fritz et al. (2003) would not have affected the magnetic properties of magnetite formed from decarbonation of siderite during an earlier impact event.

To summarize, the presence of MMC in ALH 84001 may be indicative of two different events: a) primary deposition during the initial carbonate globule-forming event in a manner similar to that seen in BVC carbonates, i.e., very rapid cooling of Fe, C, H, and O phases from hotter material in disequilibrium with the host rock (see Fig. 10); and b) formation by thermal decomposition of siderite upon heating of previously formed carbonates. In essence, however, the formation mechanisms for MMC from scenarios (a) and (b) are the same: in (a), the heat is supplied from volcanism in the case of BVC and an unknown, but probable, hydrothermal process in ALH 84001, and in (b), the heat is supplied from an impact.

The question then becomes whether both primary precipitation and impact events contribute to the formation of MMC in ALH 84001. The type 3 “ghost” globules are rings of magnetite either with or without thin carbonate films. Interestingly, they appear alongside intact carbonate globules (Fig. 1a), indicating that the spatial distribution of any heating event was heterogeneous on the scale of tens of microns. The question then becomes the following: if decarbonated, what became of the globule material? We advance the hypothesis that the small magnetite clusters within the matrix are the products of the condensation of reduced carbon, and occasionally Fe-rich carbonate, from the decarbonation of type 3 globules. Rutile associated with these structures would also help catalyze this reaction (Fig. 8e). Therefore, we advance the hypothesis that MMC produced from the thermal decomposition of siderite is found in the magnetite

assemblages of the matrix, while that found inside carbonates is from primary deposition.

Terrestrial Contamination?

Terrestrial organic contaminants have been detected in ALH 84001 (Becker et al. 1999; Jull et al. 1998; Steele et al. 2000; Stephan et al. 2003). However, it is unlikely that the MMC described in this study of ALH 84001 is contamination, as it occurs in such a spatially resolved fashion (i.e., always associated with magnetite) and within freshly revealed carbonate beneath an apparently altered outer rind. Indeed, if the externally altered rind resulted from the meteorite's residence in Antarctica for 13,000 years, then it is not unreasonable to postulate that the observed organic contamination from Antarctic ice and organisms could have become incorporated within the orange outer layer of the globules (Bada et al. 1998; Jull et al. 1998). Becker et al. (1999) found that only a small proportion (~1%) of the indigenous organic carbon in ALH 84001 is accounted for as PAHs and amino acids, while Jull et al. (1998) described a high-temperature phase of carbon, similar to MMC, that comprised approximately 20% of the carbon in the meteorite (~240 ppm). Therefore, a significant portion of the organic carbon in ALH 84001 probably exists as a macromolecular phase, and we have documented that this carbon is clearly associated with interior, fresh carbonate minerals throughout the entire depth of this meteorite. No evidence of micro-organisms was found with any MMC assemblage during SEM investigations (Steele et al. 2000). It is implausible therefore that terrestrially derived biological organic matter could account for the MMC in ALH 84001 and BVC in such a spatially resolved fashion. The similarity of the MMC in ALH 84001 to the BVC mantle MMC in peridotite carbonates, which are known to have formed from mantle fluids, supports this argument.

The Case for Biology

The formation of BVC carbonates in lherzolite xenoliths has been used to suggest liquid immiscibility in the mantle (Amundsen 1987). The carbon isotope data ($\delta^{13}C$ = –5‰) confirm a mantle origin for the BVC globules, which occur in sealed chambers within grains of olivine and pyroxene, as well as sealed within cracks between grains (Amundsen 1987). The MMC associated with these globules was deposited at the same time a CO_2- and Fe-rich mantle-derived fluid deposited magnetite, hematite, and carbonate as a single event without the influence of biology.

While we cannot completely rule out the possibility that living organisms were entrapped within the carbonate globules during their growth on Mars, we can state the following with certainty:

1. As other studies have hypothesized and we have now shown, there is an abiogenic explanation for a portion of the indigenous organic carbon in ALH 84001. These processes occur in matrix features as well as the carbonates.
2. The essence of resolving this debate (and future life detection on Mars) lies in furthering our capabilities for nanoscale detection and characterization of organic carbon. The white arrows in Fig. 9e and 9f show a 2 μm particle of magnetite surrounded by MMC. How measurements are performed on that single particle could prove or disprove whether it was the remains of a Martian organism trapped in the matrix of a carbonate globule. Currently there are no techniques that are sufficiently sensitive or spatially resolved to the extent that the biological nature of such a particle can be detected with any degree of confidence.
3. Before analysis, our experimental null hypothesis stated that all the features seen in AHL 84001 have an abiogenic origin. Based on our current research, this hypothesis could not be falsified.

Hematite in Carbonate

Several observations suggest the presence of microcrystalline hematite within ALH 84001 carbonates. These are 1) the presence of peaks within microRaman spectra indicative of hematite (Fig. 2), 2) the presence of a red-colored phase within the carbonates of the globules, and 3) the presence of a microcrystalline phase in SEM investigations of the carbonates (Figs. 9a and 9h). Laser heating studies confirm that our analytical methods were not responsible for converting siderite into hematite.

Hematite may not have been detected previously in ALH 84001 globules because the primary analytical tools were optical and electron microscopy and elemental mapping (electron microprobe, energy dispersive X-ray analysis), with the mineralogy of the carbonate composition being inferred from assessments based on the amounts of Fe, Ca, Mg, Mn, C, and O present (McKay et al. 1996; Mittlefehldt 1994a, 1994b; Mittlefehldt 1997). McSween and Harvey (1998) documented that ALH 84001 globules were predominately siderite with an unknown FeO component. Previous Raman spectroscopic studies conducted on ALH 84001 failed to detect hematite (Cooney et al. 1999; Bell et al. 1999). In the case of Cooney et al. (1999), two spectral areas of interest were selected between 150 to 800 cm^{-1} and 1000 to 1200 cm^{-1}. Bell et al. (1999) confined their area of study between 200 and 1200 cm^{-1}. Therefore neither investigation detected the strong Raman peak of hematite at ~1310 cm^{-1} peak or the ordered-disordered carbon bands of MMC (~1350 and ~1600 cm^{-1}). The lower wavenumber peaks of hematite may also have been misinterpreted as magnetite (Cooney et al. 1999). Formation of a multicarbonate (calcite, siderite,

magnesite) hematite containing globule core may have been from coprecipitation during formation, alteration over time, or from the pressure/temperature effects on primary deposited siderite of the I3 impact event. It is unclear at this time which mechanism is responsible.

Temperature of Formation

Our data are consistent with the arguments that carbonate globules in ALH 84001 formed from rapidly cooling hydrothermal Fe- and CO_2-rich fluids, principally due to their chemical and textural similarity to BVC carbonates. Treiman et al. (2002) concluded that the BVC carbonate globules formed at low temperature, postdating deposition of the zeolite mineral chabasite (Treiman et al. 2002; Treiman et al. 1998b). No zeolite minerals were detected in the carbonates studied within xenoliths. This observation combined with carbon isotope data (that shows the carbonates in basaltic vesicles formed from meteoric water and those in the xenoliths from mantle-derived fluids) indicates there are two possible populations of globules present at the BVC site. Both, however, probably formed from rapid cooling of fluids, although mantle-derived fluids would probably have a much higher initial temperature than those formed from meteoric fluids. This indicates that carbonate globules may form from fluids that vary greatly in their initial temperatures, though they may not vary much in the temperature at which deposition of the carbonate occurs. Numerous attempts to constrain the depositional temperature for carbonate globules in ALH 84001 have been undertaken by several groups (Golden et al. 2004b; Harvey and McSween 1996; Kopp et al. 2003; Leshin et al. 1998; Niles et al. 2005; Scott et al. 1998b; Scott et al. 1999; Treiman and Romanek 1998b; Valley et al. 1997a, 1997b). Each method in some way relies on knowing more than one of the many physical and chemical variables that potentially affect carbonate formation. These parameters include pressure, age, cooling rate, oxygen fugacity, pH, Eh, and cation diffusion, and have typically been calibrated against oxygen isotopic compositions. However, the oxygen isotopes of ALH 84001 have been shown to vary by over 30‰ (for review see Niles et al. 2005 and references therein). There is currently no satisfactory explanation for this variation.

Saxton et al. (1998) measured a $\delta^{18}O$ value of ~22‰ in the outer magnesite rim of ALH 84001 globules and postulated a formation temperature of 70 to 90 °C. Eiler et al. (2002) and Niles et al. (2005) have invoked a hydrothermal depositional model for the formation of carbonates in ALH 84001 as explaining the range of both carbon and oxygen isotopes found in the globules. This supports the possibility that ALH 84001 globules formed in a similar process to that of the BVC carbonates (Eiler et al. 2002; Niles et al. 2005). Niles et al. (2005), however, have criticized this idea because cooling from a higher temperature fluid would cause alteration of the host rock, and carbonate solubility would increase and not decrease in the cooling water. Alternatively, it has been shown that degassing during freezing would form similar carbonates and the fact that the globules in both ALH 84001 and BVC carbonates are slightly recessed into the host matrix (by 2–4 μM) (Fig. 1) may indicate a very localized alteration event during formation of the globules (Golden et al. 2001; Niles et al. 2004a, 2004b; Niles et al. 2006).

For accurate measurement of oxygen isotopes using an ion probe, calibration against standards of the matrix being studied is essential. In the case of ALH 84001, pure carbonate standards (Eiler et al. 1996, 1997a, 1997b; Valley et al. 1997b) were used. However, different isotopic partitioning occurring between oxygen contained in the carbonate and that in hematite may confound the oxygen isotope measurements that have been made. Therefore, to correctly interpret oxygen isotope data, a hematite-carbonate standard series, as well as pure carbonates, should be used for calibration in any measurement (Saxton et al. 1998; E. Hauri, personal communication). Saxton et al. (1998) measured shifts in $\delta^{18}O$ in a traverse across several globules. While hematite concentrations are very heterogeneous throughout the globules, our data reveal a qualitative trend of decreasing hematite concentration from center to rim (Fig. 9i). There is a qualitative trend of hematite gradient corresponding to the observed shift in $\delta^{18}O$. Therefore, revisiting this analysis with a mixed oxide phase as a calibrant may perhaps yield more consistent results (Eiler et al. 1997a).

While we favor the cooling of a hydrothermal fluid hypothesis for the formation of both the slab carbonates and Type 1 and 2 carbonate globules, we postulate that changes could have been made to ALH 84001 carbonates during a shock heating event. This may further affect the problems of interpreting the $\delta^{18}O$ composition of this rock. We suggest that future studies take into account the diverse range of globule and carbonate types in this meteorite as well as the presence of a coexisting hematite phase in the carbonates and the possibility that secondary processes have altered them.

IMPLICATIONS OF THIS WORK

We have conducted an extensive spectroscopic and imaging study of carbonates within a complete depth profile of the ALH 84001 meteorite, and compared them to mantle-derived carbonate globules from the Bockfjorden volcanic complex on Svalbard. We conclude that:

1. The microRaman peak mapping instrument used in this study is an extremely important tool in the identification of mineral species and carbon compounds in meteorites at previously unobtainable resolutions and sensitivity.
2. An outer “crust” in the ALH 84001 carbonate globules is orange and that below this layer the carbonate is white with a red/pink coloration. The outer orange layers of the carbonate may incorporate changes due to terrestrial alteration and be the repository for the organic contamination known to exist in this meteorite.

3. The zoning of carbonates in ALH 84001 is consistent with a single depositional event as shown by the BVC carbonates.
4. MMC can be produced through deposition from CO_2-rich fluids in the presence of Fe oxides. The discovery of MMC-magnetite assemblages in ALH 84001 and BVC carbonates is evidence that this formation mechanism is not restricted to terrestrial environments and cooling of CO_2-rich aqueous fluids may act as a MMC formation mechanism on any planet. This appears to be the first evidence of an abiotic MMC synthesis mechanism indigenous to Mars.
5. Both depositional and impact-induced conditions in ALH 84001 could have formed MMC, but the formation reaction mechanism for the observed MMC, i.e., cooling of CO_2-rich gases, is the same in both cases.
6. We tentatively suggest that evidence of globule decarbonation and the presence of magnetite and MMC phases in the matrix of the rock may be linked.
7. Hematite is present in all analyzed carbonates. We cannot rule out an impact shock formation mechanism for the hematite from siderite, but we suggest that it is a primary depositional phase.
8. Due to the similarity of the BVC and ALH 84001 globules, we hypothesize that the ALH 84001 globules formed in a similar manner, i.e., by cooling of hydrothermal fluids. Although we cannot constrain the temperatures at which this occurred, we suggest that further oxygen isotope analysis take into consideration the presence of an oxide phase within the siderite.
9. Our observations are consistent throughout the entire depth profile of ALH 84001.

The task of finding evidence for indigenous Martian life remains difficult. Separation of multiple carbon pools, however, is a goal that needs to be undertaken to enable life detection on Mars to advance with any reasonable degree of confidence. This study shows unequivocally, and for the first time, the existence of an abiotic MMC synthesis mechanism that is indigenous to Mars, and that the presence of MMC in ALH 84001 does not require input from chondritic carbon.

Acknowledgments–NASA SRLIDA funding (D. Lindstrom), NASA ASTEP and ASTID programs (Michael Meyer and Michael New), Marshall Scholarship program and the University of Oxford, Earth Sciences Department, NASA Astrobiology Institute and Rose Grymes. Thanks to Bevan French, Andrea Koziol, Brigitte Wopenka, Sabine Airieau, Joerg Fritz and David McKay for helpful insights. The Arctic Mars Analogue Svalbard Expedition members, in particular Alan Treiman, Lianne Benning, Bjorn Jamtveit and the crews of Polarsyssel and RV Lance, especially Otto, Meta, Morten and Corey. The staff and support of the Physics of Geological Processes (PGP) at the University of Oslo, UNIS and the Norwegian Polar Institute. In addition, the authors would like to thank Wes Huntress and Alisha Toporski for help and advice during analysis. A. Steele would also like to thank one anonymous reviewer, Tim Jull, and Cari Corrigan for their helpful advice and suggestions on making the manuscript more readable and complete.

Editorial Handling—Dr. A. J. Timothy Jull

REFERENCES

Allamandola L. J., Sanford S. A., and Wopenka B. 1988. Aromatic components in cometary materials. In *Infrared observations of comets Halley and Wilson and properties of the grains*, edited by Hanner M. S. NASA Conference Publication #2004. pp. 73–74.

Amundsen H. E. F. 1987. Evidence for liquid immiscibility in the upper mantle. *Nature* 327:692–695.

Anders E. 1991. Organic matter in meteorites and comets—Possible origins. *Space Science Reviews* 56:157–166.

Anders E., Shearer C. K., Papike J. J., Bell J. F., Clemett S. J., Zare R. N., Mckay D. S., Thomas-Keprta K. L., Romanek C. S., Gibson E. K., Jr., Vali H., Gibson E. K., Jr., McKay D. S., Thomas-Keprta K., and Romanek C. S. 1996. Evaluating the evidence for past life on Mars. *Science* 274:2119–2125.

Bada J. L., Glavin D. P., McDonald G. D., and Becker L. 1998. A search for endogenous amino acids in Martian meteorite ALH 84001. *Science* 279:362–365.

Barber D. J., Scott E. R. D., and Consolmagno G. 2001. Transmission electron microscopy of carbonates and associated minerals in ALH 84001; Impact-induced deformation and carbonate decomposition (abstract). *Meteoritics & Planetary Science* 36: A13–A14.

Barber D. J. and Scott E. R. D. 2003. Transmission electron microscopy of minerals in the Martian meteorite Allan Hills 84001. *Meteoritics & Planetary Science* 38:831–848.

Becker L., Popp B., Rust T., and Bada J. L. 1999. The origin of organic matter in the Martian meteorite ALH 84001. *Earth and Planetary Science Letters* 167:71–79.

Bell M. S., McHone J., Kudryavtsev A., and McKay D. S. 1999. Analysis of carbonates in ALH 84001 Martian meteorite by Raman spectroscopy. *GSA Abstracts with Programs* 31:45.

Bell M. S. and McKay D. S. 2000. Alteration of an ALH 84001 analog carbonate to magnetite by shock metamorphism. *GSA Abstracts with Programs* 32:240.

Brearley A. J. 2003. Magnetite in ALH 84001: An origin by shock-induced thermal decomposition of iron carbonate. *Meteoritics & Planetary Science* 38:849–870.

Clemett S. J. and Zare R. N. 1997. Microprobe two-step laser mass spectrometry as an analytical tool for meteoritic samples (abstract). International Astronomical Union Symposium 178: 305.

Clemett S. J., Dulay M. T., Gillette S., Chillier X. D. F., Mahajan T. B., and Zare R. N. 1998. Are the polycyclic aromatic hydrocarbons in ALH 84001 of extraterrestrial origin? A reevaluation (abstract #1812). 29th Lunar and Planetary Science Conference. CD-ROM.

Cooney T. F., Scott E. R. D., Krot A. N., Sharma S. K., and Yamaguchi A. 1999. Vibrational spectroscopic study of minerals in the Martian meteorite ALH 84001. *American Mineralogist* 84: 1569–1576.

Corrigan C. M. and Harvey R. 2004 Multi-generational carbonate assemblages in Martian meteorite Allan Hills 84001:

Implications for nucleation, growth, and alteration. *Meteoritics & Planetary Science* 39:17–30.

Eck R. V., Lippincott E. R., Dayhof M. O., and Pratt Y. T. 1966. Thermodynamic equilibrium and the inorganic origin of organic compounds. *Science* 153:628–633.

Eiler J. M., Graham C. M., and Valley J. W. 1996. SIMS analysis of oxygen isotopes: Matrix effects in complex minerals and glasses. *Chemical Geology* 138:221–244.

Eiler J. M., Valley J. W., Graham C. M., and Black D. 1997a. Standardization of SIMS analysis of O and C isotope ratios in carbonates from ALH 84001 (abstract). 28th Lunar and Planetary Science Conference. pp. 327–328.

Eiler J. M., Valley J. W., and Stolper E. M. 1997b. Stable isotopes in Allan Hills 84001: An ion microprobe study (abstract). *Meteoritics & Planetary Science* 32:A46.

Eiler J. M., Valley J. W., Graham C. M., and Fournelle J. 1998. Geochemistry of carbonates and glass in Allan Hills 84001 (abstract). *Meteoritics & Planetary Science* 33:A44–A45.

Eiler J. M., Valley J. W., Graham C. M., and Fournelle J. 2002. Two populations of carbonate in ALH 84001: Geochemical evidence for discrimination and genesis. *Geochimica et Cosmochimica Acta* 66:1285–1303.

Flynn G. J., Keller L. P., Jacobsen C., and Wirick S. 1998. Carbon in Allan Hills 84001 carbonate and rim (abstract). *Meteoritics & Planetary Science* 33:A50–A51.

Flynn G. J., Keller L. P., Kirz J., Wirick S., Bajt S., Chapman H. N., and Black D. 1997. Carbon mapping and carbon-XANES measurements on carbonate globules from ALH 84001 (abstract). 28th Lunar and Planetary Science Conference. pp. 365–366.

French B. M. 1971. Stability relations of siderite ($FeCO_3$) in the system Fe-C-O. *American Journal of Science* 271:37–78.

French B. M. 1965. Siderite ($FeCO_3$) thermal decomposition in equilibrium with graphite. *Science* 147:1283–1284.

Fritz J., Artemieva N., and Greshake A. 2005. Ejection of Martian meteorites. *Meteoritics & Planetary Science* 40:1393–1411.

Golden D. C., Ming D. W., Schwandt C. S., Lauer H. V., Jr., Socki R. A., Morris R. V., Lofgren G. E., and McKay G. A. 2001. A simple inorganic process for formation of carbonates, magnetite, and sulfides in Martian meteorite ALH 84001. *American Mineralogist* 86:370–375.

Golden D. C., Ming D. W., Lauer H. V., Jr., and Morris R. V. 2004a. Thermal decomposition of siderite-pyrite assemblages: Implications for sulfide mineralogy in Martian meteorite ALH 84001 carbonate globules (abstract #1396). 35th Lunar and Planetary Science Conference. CD-ROM.

Golden D. C., Ming D. W., Morris R. V., Brearley A. J., Lauer H. V., Jr., Treiman A. H., Zolensky M. E., Schwandt C. S., Lofgren G. E., and McKay G. A. 2004b. Evidence for exclusively inorganic formation of magnetite in Martian meteorite ALH 84001. *American Mineralogist* 89:681–695.

Harvey R. P. and McSween H. Y., Jr. 1996. A possible high-temperature origin for the carbonates in the Martian meteorite ALH 84001. *Nature* 382:49–51.

Hochleitner R., Tarcea, N., Simon G., Kiefer W., and Popp J. 2004. Micro-Raman spectroscopy: A valuable tool for the investigation of extraterrestrial material. *Journal of Raman Spectroscopy* 35: 515–518.

Jull A. J. T., Courtney C., Jeffrey D. A., and Beck J. W. 1998. Isotopic evidence for a terrestrial source of organic compounds found in Martian meteorites Allan Hills 84001 and Elephant Moraine 79001. *Science* 279:366–369.

Kopp R. E., Humayun M., Humayun M., and O'Neil J. R. 2003. Kinetic model of carbonate dissolution in Martian meteorite ALH 84001. *Geochimica et Cosmochimica Acta* 67:3247–3256.

Koziol A. M. 2000. Carbonate and magnetite parageneses as monitors of carbon dioxide and oxygen fugacity (abstract #1424). 31st Lunar and Planetary Science Conference. CD-ROM.

Koziol A. M. 2001. A siderite-magnesite decarbonation study. *GSA Abstracts with Programs* 33:311.

Koziol A. M. 2004. Experimental determination of siderite stability and application to Martian meteorite ALH 84001. *American Mineralogist* 89:294–300.

Leshin L. A., McKeegan K. D., Carpenter P. K., and Harvey R. P. 1998. Oxygen isotopic constraints on the genesis of carbonates from Martian meteorite ALH 84001. *Geochimica et Cosmochimica Acta* 62:3–13.

McCollom T. M. 2003. Formation of meteorite hydrocarbons from thermal decomposition of siderite ($FeCO_3$). *Geochimica et Cosmochimica Acta* 67:311–317.

McKay D. S., Gibson E. K., Jr., Thomas-Keprta K. L., Vali H., Romanek C. S., Clemett S. J., Chillier X. D. F., Maechling C. R., and Zare R. N. 1996. Search for past life on Mars: Possible relic biogenic activity in Martian meteorite ALH 84001. *Science* 273: 924–930.

McSween H. Y., Jr. and Harvey R. P. 1998. An evaporation model for formation of carbonates in the ALH 84001 Martian meteorite. *International Geology Review* 40:77–783.

Messenger S., Amari S., Gao X., Walker R. M., Clemett S. J., Chillier X. D. F., Zare R. N., and Lewis R. S. 1998. Indigenous polycyclic aromatic hydrocarbons in circumstellar graphite grains from primitive meteorites. *The Astrophysical Journal* 502:284–295.

Mittlefehldt D. W. 1994a. ALH 84001 cumulate orthopyroxenite: A previously unappreciated Martian meteorite (abstract). 20th Lunar and Planetary Science Conference. pp. 911–912.

Mittlefehldt D. W. 1994b. ALH 84001, a cumulate orthopyroxenite member of the Martian meteorite clan. *Meteoritics* 29:214–221.

Mittlefehldt D. W. 1997. Macroscopic description of Allan Hills 84001 and the relative timing of events in its history (abstract). *Meteoritics & Planetary Science* 32:A93.

Mojzsis S. J., Coath C. D, Bunch T., Blake D., Treiman A. H., and Amundsen H. E .F. 1999. Carbonate "rosettes" in xenoliths from Spitzbergen: SIMS analysis of O and C isotope ratios in a potential terrestrial analogue to Martian meteorite ALH 84001 (abstract #2032). 30th Lunar and Planetary Science Conference. CD-ROM.

Nakamura K., Zolensky M. E., Tomita S., Tomeoka K., and Warren P. H. 2002. Raman spectroscopy of carbonaceous globules in the Tagish Lake chondrite. *Meteoritics & Planetary Science* 37: A107.

Niles P. B., Leshin L. A., Socki R. A., Guan Y., Golden D. C., Ming D. W., and Gibson E. K. 2004a. Chemical and isotopic study of lab-formed carbonates under cryogenic and hydrothermal conditions (abstract #8043). Second Conference on Early Mars: Geologic, Hydrologic, and Climatic Evolution and the Implications for Life. CD-ROM.

Niles P. B., Leshin L. A., Socki R. A., Guan Y., Ming D. W., and Gibson E. K. 2004b. Cryogenic calcite—A morphologic and isotopic analog to the ALH 84001 carbonates (abstract #1459). 35th Lunar and Planetary Science Conference.

Niles P. B., Leshin L. A., and Guan Y. 2005. Microscale carbon isotope variability in ALH 84001 carbonates and a discussion of possible formation environments. *Geochimica et Cosmochimica Acta* 69:2931–2944.

Niles P. B., Zolotov M. Y., and Leshin L. A. 2006. The role of CO_2 in aqueous alteration of ultra-mafic rocks and the formation of Mg-, Fe-rich aqueous solutions on early Mars (abstract #1440). 37th Lunar and Planetary Science Conference. CD-ROM.

Pasteris J. D. and Wopenka B. 2003. Necessary, but not sufficient: Raman identification of disordered carbon as a signature of ancient life. *Astrobiology* 3:727–738.

Saxton J. M., Lyon I. C., and Turner G. 1998. Correlated chemical and isotopic zoning in carbonates in the Martian meteorite ALH 84001. *Earth and Planetary Science Letters* 160:811–822.

Scott E. R. D., Yamaguchi A., and Krot A. N. 1997a. Petrological evidence for shock melting of carbonates in the Martian meteorite ALH 84001. *Nature* 387:377–379.

Scott E. R. D., Yamaguchi A., Krot A. N., Black D., and Blanchard D. 1997b. Shock melting of carbonate, plagioclase, and silica in the Martian meteorite ALH 84001. 28th Lunar and Planetary Science Conference. pp. 1271–1272.

Scott E. R. D., Krot A. N., and Yamaguchi A. 1998. Carbonates in fractures of Martian meteorite Allan Hills 84001: Petrologic evidence for impact origin. *Meteoritics & Planetary Science* 33: 709–719.

Scott E. R. D., Krot A. N., Yamaguchi A., and Warren P. H. 1999. Petrologic evidence for low-temperature, possibly flood-evaporitic origin of carbonates in the ALH 84001 meteorite: Discussion and reply [modified]. *Journal of Geophysical Research E* 104:24,211–24,221.

Scott E. R. D., Barber D. J., and Warren P. H. 2002. Origin of magnetite in Martian meteorite Allan Hills 84001 (abstract). *Meteoritics & Planetary Science* 37:A128.

Steele A., Amundsen H. E. F., Fries M., Vicenzi E. P., Benning L., Maule J., Mysen B., Toporski J., Schweizer M., and Fogel M. 2005. A morphological and chemical study of carbonate globules contained within mantle xenoliths of the Sverrefjell volcano Spitsbergen—Implications for ALH 84001 (abstract #2173). 36th Lunar and Planetary Science Conference. CD-ROM.

Steele A., Goddard D. T., Stapleton D., Toporski J. K. W., Peters V., Bassinger V., Sharples G., Wynn-Williams D. D., and McKay D. S. 2000. Investigations into an unknown organism on the Martian meteorite Allan Hills 84001. *Meteoritics & Planetary Science* 35:237–241.

Stephan T., Jessberger E. K., Heiss C. H., and Rost D. 2003. TOF-SIMS analysis of polycyclic aromatic hydrocarbons in Allan Hills 84001. *Meteoritics & Planetary Science* 38:109–116.

Treiman A. H. 1995. A petrographic history of Martian meteorite ALH 84001: Two shocks and an ancient age. *Meteoritics* 30:294–302.

Treiman A. H. 1998a. The history of Allan Hills 84001 revised: Multiple shock events. *Meteoritics & Planetary Science* 33:753–764.

Treiman A. H. and Romanek C. S. 1998b. Bulk and stable isotopic compositions of carbonate minerals in Martian meteorite Allan Hills 84001: No proof of high formation temperature. *Meteoritics & Planetary Science* 33:737–742.

Treiman A. H., Amundsen H. E. F., Blake D. F., and Bunch T. 2002. Hydrothermal origin for carbonate globules in Martian meteorite ALH 84001: A terrestrial analogue from Spitsbergen (Norway). *Earth and Planetary Science Letters* 204:323–332.

Treiman A. H. 2003. Submicron magnetite grains and carbon compounds in Martian meteorite ALH 84001: Inorganic, abiotic formation by shock and thermal metamorphism. *Astrobiology* 3: 369–392.

Valley J. W., Eiler J. M., Graham C. M., Gibson E. K., Jr., Romanek C. S., Black D., and Blanchard D. 1997a. Ion microprobe analysis of oxygen and carbon isotope ratios in the ALH 84001 (abstract). 28th Lunar and Planetary Science Conference. pp 1475–1476.

Valley J. W., Eiler J. M., Graham C. M., Gibson E. K., Jr., Romanek C. S., and Stolper E. M. 1997b. Low-temperature carbonate concretions in the Martian meteorite ALH 84001: Evidence from stable isotopes and mineralogy. *Science* 275:1633–1638.

Wang A., Kuebler K., Jolliff B., and Haskin L. A. 2004a. Mineralogy of a Martian meteorite as determined by Raman spectroscopy. *Journal of Raman Spectroscopy* 35:504–514.

Wang A., Kuebler K. E., Jolliff B. L., and Haskin L. A. 2004b. Raman spectroscopy of Fe-Ti-Cr-oxides, case study: Martian meteorite EETA79001. *American Mineralogist* 89:665–680.

Weidner P. H. 1972. Equilibria in the system Fe-C-O. I—siderite-magnesite-carbon vapor equilibrium from 500–10,000 bars. *American Journal of Science* 272:735–751.

Weiss B. P., Kirschvink J. L., Baudenbacher F. J., Vali H., Peters N. T., MacDonald F. A., and Wikswo J. P. 2000. A low-temperature transfer of ALH 84001 from Mars to Earth. *Science* 290:791–795.

Weiss B. P., Vali H., Baudenbacher F. J., Kirschvink J. L., Stewart S. T., and Shuster D. L. 2002. Records of an ancient Martian magnetic field in ALH 84001. *Earth and Planetary Science Letters* 201:449–463.

Wopenka B. and Swan P. D. 1985. Identification of micron-sized phases in meteorites by laser Raman microprobe spectroscopy (abstract). *Meteoritics* 20:788–789.

Zolotov M. Y. and Shock E. L. 2000. An abiotic origin for hydrocarbons in the Allan Hills 84001 Martian meteorite through cooling of magmatic and impact-generated gases. *Meteoritics & Planetary Science* 35:629–638.